

RSC Advances



This is an *Accepted Manuscript*, which has been through the Royal Society of Chemistry peer review process and has been accepted for publication.

Accepted Manuscripts are published online shortly after acceptance, before technical editing, formatting and proof reading. Using this free service, authors can make their results available to the community, in citable form, before we publish the edited article. This *Accepted Manuscript* will be replaced by the edited, formatted and paginated article as soon as this is available.

You can find more information about *Accepted Manuscripts* in the [Information for Authors](#).

Please note that technical editing may introduce minor changes to the text and/or graphics, which may alter content. The journal's standard [Terms & Conditions](#) and the [Ethical guidelines](#) still apply. In no event shall the Royal Society of Chemistry be held responsible for any errors or omissions in this *Accepted Manuscript* or any consequences arising from the use of any information it contains.

A green, rapid and size-controlled production of high-quality graphene sheets by hydrodynamic forces

Lei Liu,^{ac} Zhigang Shen,^{*ab} Min Yi,^{ab} Xiaojing Zhang^a and Shulin Ma^a

Based on hydrodynamics mechanism, a novel, scalable and rapid production of relatively defect-free graphene nanosheets (GNSs) by high shear mixer is proposed in this paper. The synergistic enhancement of shear forces and collision effects can result in an effective exfoliation of ultrathin GNSs. Besides, the productivity and dimension distribution of GNSs can be easily controlled by adjusting hydrodynamic forces. Utilizing the small stator, the concentration of mono- and multilayer GNSs prepared for 1 h in 40 vol % IPA-water mixtures can reach 0.27 mg ml⁻¹. Almost all of GNSs are less than 1 μm in average size and 2 nm in thickness. Furthermore, the mixtures of isopropanol (IPA) and water are low boiling, green, cheap, and have excellent solubility of GNSs. The optimum volume fraction of IPA-water mixtures for preparing GNSs is codetermined by Hansen solubility parameter distance (Ra), surface tension and the viscosity. More importantly, graphite particles have strong physical interaction with hydrodynamic forces, but GNSs structure also can keep relatively defect-free. Consequently, this scalable, rapid and high-yield method can be well applied in the production of GNSs and other two-dimensional (2D) materials.

Introduction

Graphene, a 2D special layered nano-material with various novel and excellent properties, has attracted great interests because it has potential applications in numerous fields.¹⁻³ There are a variety of methods have been proposed for GNSs production, including micromechanical exfoliation,⁴ chemical vapor deposition,⁵ reduction of graphene oxide,⁶ arc discharge in air,⁷ intercalative expansion of graphite and liquid-phase exfoliation.^{8,9} Graphene oxide flakes are obtained by interlayer oxidation and can be reduced by many methods, but massive structure defects obviously reduce the material performances.⁶ A dispersion containing about 0.3 mg ml⁻¹ GNSs have been prepared by sonication over 400 h, and sonication mostly depends on cavitation effect to exfoliate graphite. But cavitation effects are commonly induced in the limited area near the ultrasonic generator, resulting in a low efficiency.¹⁰ The scalable production of mono- and multilayer GNSs by media mill indicates that GNSs can be delaminated by using pure mechanical forces.¹¹

Large-scale GNSs are regarded as a desirable material for preparing transparent conductive films, biological sensing, nanoelectronic devices and composites materials.¹²⁻¹⁵ However, small GNSs (less than 1 μm) also possess strong potential for biomedicine, sensors, optoelectronic devices and transparent conductive films.¹⁶⁻¹⁹ In particular, small GNSs can be printed onto flexible plastic surfaces to prepare novel conductive films by inkjet technique which is one of the most promising techniques for industrial application.¹⁹⁻²¹ But small GNSs are difficult to be produced and separated, which limits their wide application. At present, the main preparation methods are: chemical cutting, mechanically grinding and density gradient ultracentrifugation rate.²²⁻²⁴ But these methods have some drawbacks, such as structure destruction, properties reduction, low efficiency or high cost. It should be noted the massive defects of band structure can obviously reduce the electrical conductivity of GNSs. In order to overcome these limitations and obtain high-quality graphene, we developed a novel, rapid and effective route to exfoliate graphite particles into small and high-quality GNSs in this paper, and a comparison is given in Tab. S1 (see ESI†).

High shear mixer is also called rotor stator mixer and it has been widely used in pulverization and emulsification.^{25,26} The typical characteristics of high shear mixer are narrow gap between the rotor and stator (100-3000 μm), high rotor speed (10-50 m s⁻¹) and high shear rate (20,000-100,000 s⁻¹).²⁷ The working mechanisms of high shear mixer base on the hydrodynamics and can be divided into high shear force, collision effects and jet cavitation.²⁸ Rapid and violent fluid produces strong physical interaction with graphite particles, which is sufficient to overcome Van der Waals forces between layers. Recently, the group of Coleman report the production of two-dimensional nano-materials by high shear method in organic solvent, surfactant and polymer solutions.²⁹ They considered the turbulence to be unnecessary for exfoliation and the high shear is the chief force. A simple exfoliation model, shear-induced interlayer sliding in a solvent, was used to predict a minimum shear rate to produce graphene. However, hydrodynamic forces of high shear mixers is complex, including shear force, collision effects and cavitation, and difficult to use a simplified model to accurately simulation. Hence, the effects of shear force and collision on exfoliating of GNSs was further investigated in this paper.

It is accepted that N-methyl-2-pyrrolidone (NMP) and dimethylformamide (DMF) are excellent solvents for preparing GNSs. but they are expensive, high boiling and toxic. The surfactant solutions easily lead to residue in products. In addition, most cheap, green and low-boiling solvents have unsatisfying solubility of GNSs. Hansen solubility parameters (HSP) has been used for roughly predicting the solubility of materials in solvents.^{30,31} The mixtures of several poor solvents have been shown to be effective solutions which have extremely high dissolving capacity by achieving the adaptation between the HSP parameters of mixtures and material.³² Particularly, IPA is a high viscosity, low boiling and green solvent which is singularly appropriate to be utilized to investigate the effects of solution parameters on the production of GNSs by hydrodynamic forces.

In the present article, we demonstrate a scalable and high-efficiency hydrodynamics method to prepare GNSs in IPA-water mixtures. Using violent and multiple hydrodynamic forces, the graphite particles can be rapidly and effectively exfoliated into small GNSs. Besides, IPA-water mixtures show excellent dissolution behaviour for GNSs, and are used to analyse the effects of Ra, surface tension

and the viscosity on the preparation of GNSs. Interestingly, the viscosity is considered a vital factor in the hydrodynamic exfoliation of GNSs. Above all, GNSs prepared with small stator for 1h are less than 1 μm in average size and 2 nm in thickness, exhibiting a broad prospect in industrial applications. In summary, this hydrodynamics-assisted method involving various exfoliation mechanisms realizes a high yield and efficiency production of GNSs and has great potential in the exfoliation of other layered materials.

Experimental

The graphite powder used in these experiments was purchased from Alfa Aesar (Product Number 43209). The graphite particles were dispersed in the required solvent (DMF or IPA-water mixtures) at a concentration of 5 and 10 mg ml^{-1} . These dispersions were treated in a stainless steel cylinder (about 10 cm in diameter) at the maximum speed (about 9500 rpm) by high shear mixer (FM300, Fluko, China). The temperature of dispersions was controlled at the low temperature (about 20 $^{\circ}\text{C}$) by cooling water. Without the cooling system, the solvent might get hot quickly and then evaporated, which obviously affect the production of GNSs. The dispersions were centrifuged at 450 rpm for 45 min in a centrifuge machine (L600, Xiangyi, China). After centrifugation, the supernatant was carefully removed and retained for further use.

Samples of GNSs for SEM analysis were prepared by vacuum filtering the dispersions onto porous membranes and were dried for 24 h in 60 $^{\circ}\text{C}$. AFM and TEM specimens were prepared by dropping a few diluting suspension onto the mica and the holey carbon mesh grid or ultrathin carbon support film, respectively. FESEM and SEM images were obtained using Apollo 300 and CS3400 (CamScan, England), respectively. TEM images were taken with a JEM-2100 (JEOL, Japan). The thickness and size of GNSs were obtained using Bruker MultiMode 8 which was used in ScanAsyst Air mode. Raman spectroscopy was carried out on Rm2000 instrument (Renishaw, England) using 514 nm laser excitation. The optical absorbance of the final suspension was determined using TU-1901 (Purkinje, China) at a wavelength of 660 nm, and the GNSs concentration was obtained according to Lambert-Beer law.³³ The surface tension is determined using SFT-C1 surface tensiometer (HARKE, China). The viscosity of solvents was obtained by Ubbelohde viscometer at 25 ± 0.1 $^{\circ}\text{C}$.

Results and discussion

Graphite particles can be regarded as a set of GNSs stacked orderly and held together by van der Waals forces. The interaction energy of graphite particle is relatively weak, therefore the delamination of graphite particles can be realized by various sufficiently high forces in theory, such as shear force, shock wave, micro jet, collision, and so on.^{11,34} Utomo et al. performed computational fluid dynamics to investigate the distribution of energy dissipation of high shear mixer. The main energy dissipated regions can be divided into rotor swept region, hole region and jet region, which can be roughly regarded as corresponding to shear force, edge collision and jet cavitation, respectively (Fig. 1b).³⁵

By wet grinding, GNSs which are less than 1.5 μm in the lateral size can be peeling off by shear force transferred from the milling beads.¹¹ Additionally, graphene nanodots also can be detached from particles using pure shear force and have an average size of 9-29 nm for different times.³⁶ It is important to note that small sheets are easier to be peeled from the particle surface than larger ones because of the smaller collective interaction force between layers. Therefore ultrathin sheets may be easily torn on the edge by shear force and may tend to become relatively small-scaled (Fig. 1c). Fig. 1a shows the detail of high shear generator which consists of the stator and the rotor, and additional photographs of different stators are shown in Fig. S1 (see ESI[†]). The blades of the rotor run at high speeds and expel the solvents into the surrounding space, resulting in high speed fluid flows in the narrow gap between the stator and the rotor. High shear force can easily be induced by large velocity gradient of the fluid. Above all, high viscous shear force induced by fluid flow can directly act on the weak interface of layers of particles, resulting in high efficient.

In addition, when high speed fluid jets out from drain holes of the stator, jet cavitation could be induced by high pressure difference due to abrupt velocity change and geometrical change.³⁷ Cavitation have been proved to be an effective way to prepare GNSs on account of shock waves and micro jets.³⁸ Nevertheless the drain holes are too large to generate enough high pressure difference for cavities growth and bubble implosion, so the jet cavitation may play a minor role in the GNSs production.³⁹ Moreover, as a weak force for exfoliating graphite particles, collision effects are frequently overlooked, but it may be the principal force of high shear mixer. High energy dissipation had been proved to occur around the leading edges of drain holes,⁴⁰ thus the graphite particles may be subjected to the tremendous collision when the dispersion periodically and rapidly impinged on the hole edges.⁴⁰ The frequent and random collisions between graphite particles also can occur by extremely large inertial force in the turbulence region. The serious pileups of graphite particles can lead to graphite particles self-exfoliation down to mono- and multilayer GNSs (Fig. 1c). Interestingly, curl, loose and thin layers replaced the orderly and thick ones at the edge of graphite particles, where strong and sudden shocks caused serious deformation (Fig. S2, see ESI). This destruction can conduce to synergistically reinforce the exfoliating effects of shear forces. These frequent and violent collisions greatly accelerate the exfoliation and, most importantly, the size of GNSs can sharply decrease.

IPA-water mixtures with different volume fraction have distinctive surface tensions, viscosities and Ra values. It has been proven that surface tension and Ra is closely related to the solubility of GNSs in different solvents.²⁸ For minimal energy cost of exfoliation, the optimum surface energy of solvents need to match that of GNSs and the surface tension of excellent solvents mainly concentrate in the region of 40-50 mJ m^{-2} .³³ The surface tension of 10 vol % IPA-water mixtures (about 42.5 mJ m^{-2}) is located in this optimum range (grey area in Fig. 2a), but actually 40 vol % IPA-water solution can achieve the highest concentration. For another,

HSP theory is an important tool to analyze the solubility of materials in solvents.^{32,41} R_a can be calculated from the dispersive, polar, and hydrogen-bonding solubility parameters (see ESI†). The dissolving capacity normally improves with the decrease of R_a values. Compared with the optimum volume fraction (10 vol %) of IPA predicted by the surface energy, the minimum point (65 vol %) of R_a curve is close to 40 vol % at which the highest concentration can be achieved (Fig.2).

To further analyze the reason which causes the change of the optimum proportion, we compared the stability of GNSs dispersions with the same GNSs concentration (about 0.195 mg ml⁻¹) but different volume fractions of IPA. To avoid the effect of different sizes and thicknesses of GNSs, all dispersions were diluted from a dispersion containing 80 vol % IPA after 500 rpm centrifugation. The C/C_T values can directly represent the stability of these dispersions. After standing for one month at room temperature, 40 vol %, 50 vol % and 60 vol % dispersions showed the satisfactory stability. Besides, the stability of GNSs dispersions can reflect the solubility of GNSs in these solutions. The results of the stability are approximating consistent with the theoretical result calculated by HSP theory. But the mixtures containing low volume fraction of IPA showed better dissolving capacity than that of prediction by Hansen theory because of relatively high surface energy. Above all, the stability curve is similar to the C_G curve, indicating the exfoliating effects of GNSs dispersions are obviously influenced by the dissolving of solvents.

Viscosity of solvents is another important parameter in hydrodynamics, which can influence the motion of the liquid layer. By decreasing the viscosity of solvents, the shear force may be reduced as a result of the decrease of the velocity gradient. DMF is a perfect solvent for preparing graphene by sonication and have a low R_a value (about 6.76) and a certain surface tension (34.4 mN m⁻¹ in 25°C), but it has lower viscosity (0.802 mPa·s in 25°C) than IPA (1.96 mPa·s in 25°C) and most IPA-water mixtures (Fig. 2).⁴² The concentration of GNSs dispersion prepared in DMF is about 0.06 mg ml⁻¹, which is far lower than that of prepared in 40 vol % IPA-water mixture (about 0.27 mg ml⁻¹). Similarly, using 0.1 mg ml⁻¹ surfactant solution (sodium dodecyl benzene sulfonate, SDBS) which viscosity is close to pure water, GNSs dispersion obtained under the same condition is less than 0.01 mg ml⁻¹. Hence relatively high viscosity is beneficial to preparing of GNSs by high shear mixer. Consequently, the best experimental volume fraction is about 40 vol % which is located among the optimum values of surface tension, the viscosity and R_a , illustrating that various factors can contribute to GNSs production. At the optimum mixing ratio, the graphene concentration is obviously higher than that in single water and IPA, which indicates mixed strategy can change poor solvents into effective ones.]

As shown in Fig. 2b, GNSs concentration increases with prolonging the treating time. Besides, the concentration curve can be approximately divided into two regions with different growth rates. In initial phase, the concentration rapidly increases because the delamination and cleavage of large pristine particles. With the continual decrease of the lateral size and thickness of graphite particles, the growth of GNSs concentration slows down. Besides, the effects of hydrodynamic force can be controlled by changing the gap between the rotor and the stator. The concentration of GNSs dispersion prepared with small stator is about 2.7 times as high as that of the large stator dispersion (Fig. 2b). High initial concentration of graphite particles also has an advantage on preparing GNSs in that collision effects can be enhanced with increasing number of particles.

Fig 3a, b shows a comparison of pristine graphite and the sediment. Most pristine graphite particles are ellipsoid shape and characterized as a typical layering structure. In contrast, the sediment became relatively small and thin flakes after treatment, indicating the adequate exfoliation of graphite particles occurred under violent hydrodynamics conditions. Obviously, a large number of thin GNSs can be peeled from the surfaces of graphite particles in this process. Fig.3c, d show GNSs with different sizes are thin, curly and transparent, which reveals the graphite particles were successful exfoliated. Importantly, GNSs prepared with small stator is smaller than that of large stator sample.

Atomic force microscopy (AFM) is one of the most direct and precise methods for observing and analysing the micro-topography of 2D nanosheets. Fig.4a, b show the significant difference between small and larger stators samples. The mean size of GNSs treated with small stator is much smaller than that prepared with large stator. The height scale of GNSs is about 1nm (Fig. 4b), which can be generally considered as monolayer or bi-layers graphene due to the negative influences of the residual solvent and the roughness of mica surface.⁴³ TEM can further characterize the flakes in the dispersions. The restacking of some individual GNSs with the lateral size of 50- 500 nm was observed (Fig. 4c). Similarly, Fig. 4d displays large GNSs adhered with each other. These results can further confirm the obvious change of GNSs size by adjusting the size of the gap.

By analysis of AFM images of GNSs, we can investigate the effects of the gap size on the thickness and size of GNSs. Fig.4e shows the histograms of thickness and average size (average value of the width and the length) by analysing approximately 1000 flakes. Additional AFM images are available in Fig. S3 (see ESI†). The mean thickness and average size of GNSs prepared with large stator are 1.3 nm and 0.9 μm, respectively. Using the small stator, the mean thickness and average size decreased to 0.9nm and 0.35 μm, respectively. Above all, more than 94 % of sheets prepared with small stator are smaller than 450 nm, but only 29 % for the large stator. 62 % of GNSs are thinner than 1 nm and nearly all sheets are below 2.5 nm when the small stator is used. It is apparent that GNSs tend to be thin and small under violent hydrodynamic forces as decreasing the gap size.

Representative Raman spectrums of GNSs and pristine graphite are shown in Fig.5a. Compared with graphite particles, significant changes of the G band (~1570 cm⁻¹), the 2D band (~2690 cm⁻¹) and the D band (~1350 cm⁻¹) can be observed in GNSs spectrums. The emergence of D band is mainly induced by structure defects, the diffusion of structural disorder and the edge disturbance.^{44, 45} In particular, the edge disturbance might be the largest contributor to the presence of D band because GNSs (less than 2 μm in lateral dimensions) can be covered by the laser point (1 ~ 2 μm in diameter). Meanwhile, the intensity proportion of D band to G band (I_D/I_G) can simply represent the damage of structure. The intensity ratios I_D/I_G of GNSs prepared with large and small stators are about 0.14 and 0.18, which are much lower than that of GO and GNSs prepared by sonication.^{46, 47} Because the chemical interaction induced by

shear force and collision is obviously weaker than that induced by sonication effects which generate temperatures of about 4000 K and pressures in excess of 1000 atmospheres in a small region of space.⁴⁸ The G bands do not obviously present pronounced broadening, further indicating that the structural disorder defects in basal plane is negligible. Less destruction is beneficial to maintaining the excellent properties of GNSs. To further investigate the defects of GNSs, X-ray photoelectron spectroscopy (XPS) characterization was carried out. In Fig. 5b, the C1s XPS spectra of the delaminated GNSs which were prepared by high shear mixers with small stator are presented. The C1s spectrum of GNSs clearly shows the binding energy feature at 284.8 eV corresponding to the graphitic carbon (C -C). However, a number of smaller features are also observed at 285.7 eV and 287.2 eV which is typically assigned to C-O and C=O, which is similar with that prepared by media mill.¹¹ In contrast with reduce graphene oxide, these features are lower.³ The residual solvent also might result in the observable oxidization of GNSs. Hence, these indicates that few oxygenous defects in GNSs prepared by high shear mixer.

We can measure the stability of GNSs dispersions by monitoring the dispersion concentration optically, which was performed after standing one day to remove big and thick particles. Typical sedimentation curves of GNSs dispersions are shown in Fig.5c. Compared with the large stator sample, a slow and relatively steady sedimentation was observed in the case of small stator and this tended to be stable after about 25 days. The small and thin GNSs have higher stability owing to high edge effects.⁴⁹ At the same concentration, a comparison of the sedimentation of two different dispersions is shown in Fig.5c. Obvious change of transparent occurred in the large stator sample, indicating the small GNSs are propitious to preservation and further application.

Conclusions

A novel, rapid and effective method for small GNSs production which involves multiple hydrodynamic forces was demonstrated in this research. The exfoliating effectiveness is influenced by Ra value, the surface tension and the viscosity of the mixtures. In addition, the GNSs concentration can be significantly improved by extending the treating time and increasing the initial concentration. Above all, the thickness and size of GNSs can be controlled by changing the gap size. Using the small stator, we have successfully prepared small GNSs, 95% of sheets possess lateral sizes ranging from 0 to 450 nm. And approximate 62% of nanosheets are less than 1nm thick and only a minority with more than 2nm thick are observed. Furthermore, XPS and Raman spectroscopy show that GNSs are relatively free of structure defects. It can be anticipated that this novel and scalable exfoliating mechanism will extend new way for liquid-phase production of other layered materials, including MoS₂ and BN besides graphite, in green and user-friendly solutions.

Acknowledgements

This work was funded by Beijing Natural Science Foundation (Grant No. 2132025), the Special Funds for Co-construction Project of Beijing Municipal Commission of Education, and the Fundamental Research Funds for the Central Universities, the Specialized Research Fund for the Doctoral Program of Higher Education (Grant No. 20131102110016)

Notes and references

^a Beijing Key Laboratory for Powder Technology Research and Development, Beijing University of Aeronautics and Astronautics, Beijing 100191, China. E-mail: shenzhg@buaa.edu.cn;

^b Ministry of Education Key Laboratory of Fluid Mechanics, Beijing University of Aeronautics and Astronautics, Beijing 100191, China

^c School of Material Science and Engineering, Beijing University of Aeronautics and Astronautics, Beijing 100191, China

† Electronic Supplementary Information (ESI) available: [details of any supplementary information available should be included here]. See DOI: 10.1039/b000000x/

1. E. Voloshina and Y. Dedkov, *Phys. Chem. Chem. Phys.*, 2012, **14**, 13502-13514.
2. G. Zhao, T. Wen, C. Chen and X. Wang, *RSC Advances*, 2012, **2**, 9286-9303.
3. S. Mao, H. Pu and J. Chen, *RSC Advances*, 2012, **2**, 2643-2662.
4. K. Novoselov, A. K. Geim, S. Morozov, D. Jiang, Y. Zhang, S. Dubonos, I. Grigorieva and A. Firsov, *Science*, 2004, **306**, 666-669.
5. A. Ambrosi, A. Bonanni, Z. Sofer and M. Pumera, *Nanoscale*, 2013, **5**, 2379-2387.
6. Q. He, H. G. Sudibya, Z. Yin, S. Wu, H. Li, F. Boey, W. Huang, P. Chen and H. Zhang, *Acs Nano*, 2010, **4**, 3201-3208.
7. Z. Wang, N. Li, Z. Shi and Z. Gu, *Nanotechnology*, 2010, **21**, 175602.
8. L. Niu, M. Li, X. Tao, Z. Xie, X. Zhou, A. P. A. Raju, R. J. Young and Z. Zheng, *Nanoscale*, 2013, **5**, 7202-7208.
9. M. Lotya, P. J. King, U. Khan, S. De and J. N. Coleman, *ACS nano*, 2010, **4**, 3155-3162.
10. J. M. Englert, J. Röhrl, C. D. Schmidt, R. Graupner, M. Hundhausen, F. Hauke and A. Hirsch, *Adv. Mater.*, 2009, **21**, 4265-4269.
11. C. Knieke, A. Berger, M. Voigt, R. N. K. Taylor, J. Röhrl and W. Peukert, *Carbon*, 2010, **48**, 3196-3204.
12. X. An and J. C. Yu, *RSC Advances*, 2011, **1**, 1426-1434.
13. Z. Wang, H. Zhang, N. Li, Z. Shi, Z. Gu and G. Cao, *Nano Research*, 2010, **3**, 748-756.

14. P. T. Yin, T.-H. Kim, J.-W. Choi and K.-B. Lee, *Phys. Chem. Chem. Phys.*, 2013, **15**, 12785-12799.
15. Q. Su, S. Pang, V. Aljani, C. Li, X. Feng and K. Müllen, *Adv. Mater.*, 2009, **21**, 3191-3195.
16. M. Zhang, L. Bai, W. Shang, W. Xie, H. Ma, Y. Fu, D. Fang, H. Sun, L. Fan and M. Han, *J. Mater. Chem.*, 2012, **22**, 7461-7467.
17. V. Gupta, N. Chaudhary, R. Srivastava, G. D. Sharma, R. Bhardwaj and S. Chand, *J. Am. Chem. Soc.*, 2011, **133**, 9960-9963.
18. H. Razmi and R. Mohammad-Rezaei, *Biosens. Bioelectron.*, 2013, **41**, 498-504.
19. F. Torrisi, T. Hasan, W. Wu, Z. Sun, A. Lombardo, T. S. Kulmala, G.-W. Hsieh, S. Jung, F. Bonaccorso and P. J. Paul, *Acs Nano*, 2012, **6**, 2992-3006.
20. Y. Yu, H. Wada, J.-i. Inoue, S. Imaizumi, Y. Kounosu, K. Tsuboi, H. Matsumoto, M. Ashizawa, T. Mori and M. Minagawa, *Appl. Phys. Express*, 2011, **4**, 115101.
21. L. Huang, Y. Huang, J. Liang, X. Wan and Y. Chen, *Nano Research*, 2011, **4**, 675-684.
22. D. Pan, J. Zhang, Z. Li and M. Wu, *Adv. Mater.*, 2010, **22**, 734-738.
23. G. P. Kotchey, B. L. Allen, H. Vedala, N. Yanamala, A. A. Kapralov, Y. Y. Tyurina, J. Klein-Seetharaman, V. E. Kagan and A. Star, *ACS nano*, 2011, **5**, 2098-2108.
24. X. Sun, D. Luo, J. Liu and D. G. Evans, *ACS nano*, 2010, **4**, 3381-3389.
25. P. Ding, M. Orwa and A. Pacey, *Powder Technol.*, 2009, **195**, 221-226.
26. W. Xu, B. Gao, Q. Yue and Y. Wang, *Water Res.*, 2010, **44**, 1893-1899.
27. E. L. Paul, V. Atiemo-Obeng and S. M. Kresta, *Handbook of industrial mixing: science and practice*, Wiley. com, 2004.
28. J. A. Gantt and E. P. Gatzke, *Powder Technol.*, 2005, **156**, 195-212.
29. K. R. Paton, E. Varrla, C. Backes, R. J. Smith, U. Khan, A. O'Neill, C. Boland, M. Lotya, O. M. Istrate and P. King, *Nature Mater.*, 2014, **13**, 624-630.
30. S. D. Bergin, Z. Sun, P. Streich, J. Hamilton and J. N. Coleman, *J. Phys. Chem. C*, 2009, **114**, 231-237.
31. Y. Hernandez, M. Lotya, D. Rickard, S. D. Bergin and J. N. Coleman, *Langmuir*, 2009, **26**, 3208-3213.
32. K. G. Zhou, N. N. Mao, H. X. Wang, Y. Peng and H. L. Zhang, *Angew. Chem. Int. Edit.*, 2011, **50**, 10839-10842.
33. Y. Hernandez, V. Nicolosi, M. Lotya, F. M. Blighe, Z. Sun, S. De, I. McGovern, B. Holland, M. Byrne and Y. K. Gun'ko, *Nat. Nanotech.*, 2008, **3**, 563-568.
34. W. Choi, I. Lahiri, R. Seelaboyina and Y. S. Kang, *Crit. Rev. Solid State*, 2010, **35**, 52-71.
35. A. T. Utomo, M. Baker and A. W. Pacey, *Chem. Eng. Res. Des*, 2008, **86**, 1397-1409.
36. N. G. Shang, P. Papakonstantinou, S. Sharma, G. Lubarsky, M. Li, D. W. McNeill, A. J. Quinn, W. Zhou and R. Blackley, *Chem. Commun.*, 2012, **48**, 1877-1879.
37. Z. Shen, J. Li, M. Yi, X. Zhang and S. Ma, *Nanotechnology*, 2011, **22**, 365306.
38. U. Khan, H. Porwal, A. O'Neill, K. Nawaz, P. May and J. N. Coleman, *Langmuir*, 2011, **27**, 9077-9082.
39. B. Ran and J. Katz, *J. Fluid. Mech.*, 1994, **262**, 223-263.
40. A. Utomo, M. Baker and A. Pacey, *Chem. Eng. Res. Des*, 2009, **87**, 533-542.
41. M. Yi, Z. Shen, X. Zhang and S. Ma, *J. Phys. D: Appl. Phys.*, 2013, **46**, 025301.
42. C. L. Yaws, McGraw-Hill, New York, 1999.
43. P. Nemes-Incze, Z. Osváth, K. Kamarás and L. Biró, *Carbon*, 2008, **46**, 1435-1442.
44. A. Ferrari, J. Meyer, V. Scardaci, C. Casiraghi, M. Lazzeri, F. Mauri, S. Piscanec, D. Jiang, K. Novoselov and S. Roth, *Phys. Rev. Lett.*, 2006, **97**, 187401.
45. D. Graf, F. Molitor, K. Ensslin, C. Stampfer, A. Jungen, C. Hierold and L. Wirtz, *Nano Lett.*, 2007, **7**, 238-242.
46. A. O'Neill, U. Khan, P. N. Nirmalraj, J. Boland and J. N. Coleman, *J. Phys. Chem. C*, 2011, **115**, 5422-5428.
47. G. K. Ramesha and S. Sampath, *J. Phys. Chem. C*, 2009, **113**, 7985-7989.
48. K. Yasui, T. Tuziuti, Y. Iida and H. Mitome, *J. Chem. Phys.*, 2003, **119**, 346-356.
49. M. Yi, Z. Shen, S. Liang, L. Liu, X. Zhang and S. Ma, *Chem. Commun.*, 2013, **49**, 11059-11061.

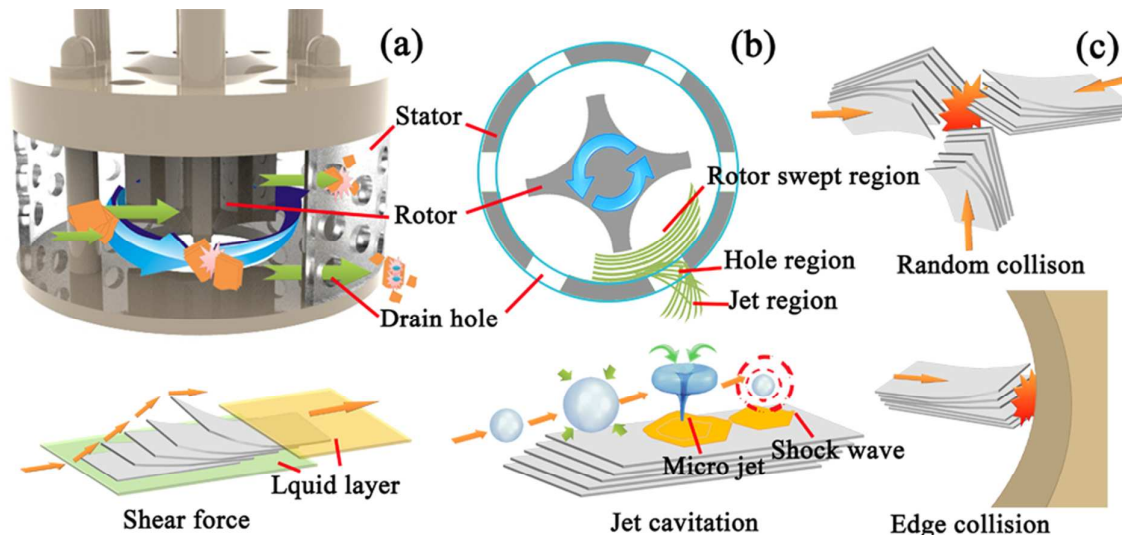


Fig. 1 (a) 3D sectional drawing of the high shear generator; (b) Main energy dissipation regions of the high shear mixer (sectional view); (c) The schematic model of preparing GNSs by shear force, collision and jet cavitation.

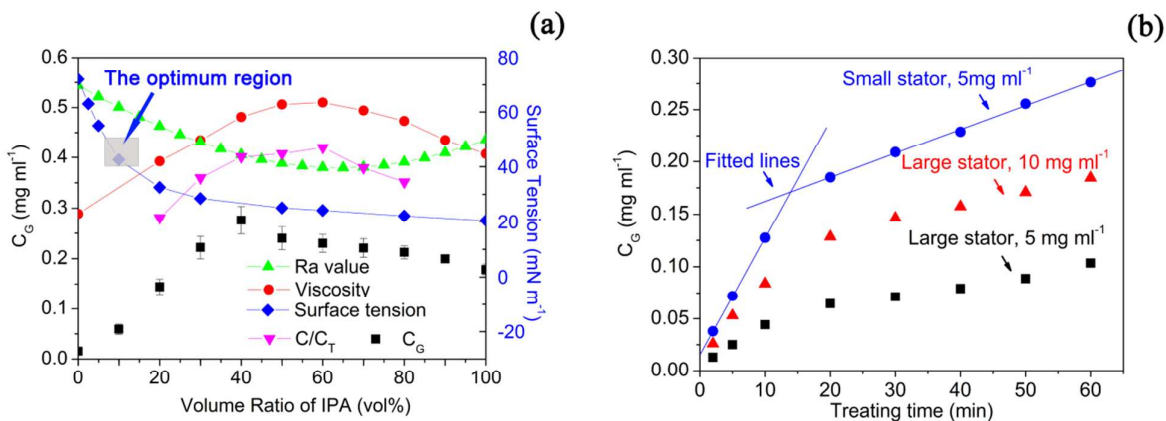


Fig. 2 (a) Graphene concentration (C_G), viscosity, surface tension and Ra value of IPA-water mixtures with different volume fraction. The grey area presents the optimum region of surface tension. C/C_T is the residual concentration after standing for one month to the initial concentration. (b) The concentration of GNSs dispersion prepared with different stators in 40 vol % IPA-mixtures. Fitted lines of CG show the different growth rates in the initial and relatively steady phases.

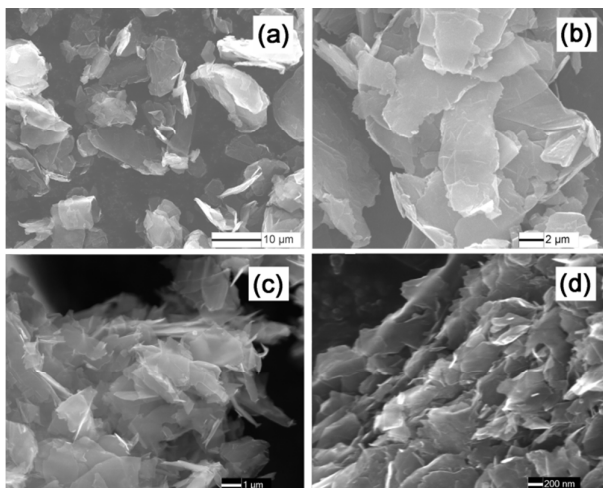


Fig. 3 SEM images of (a) pristine graphite particles, (b) the sediment. FESEM image of GNSs prepared with (c) the large and (d) the small stators.

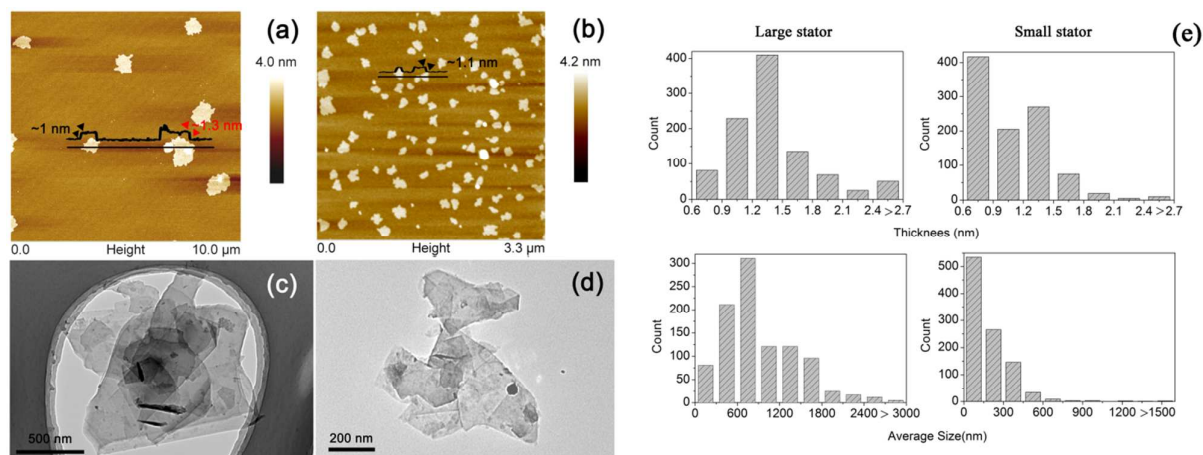


Fig. 4 AFM and TEM images of GNSs prepared with (a, c) large and (b, d) small stators. To avoid the loss of small flakes through the holes in the holey carbon grid, the small stator sample was prepared in ultrathin carbon support film. (e) Statistical analysis of AFM images showing histograms of thickness and flake average size for GNSs dispersion prepared with large and small stators.

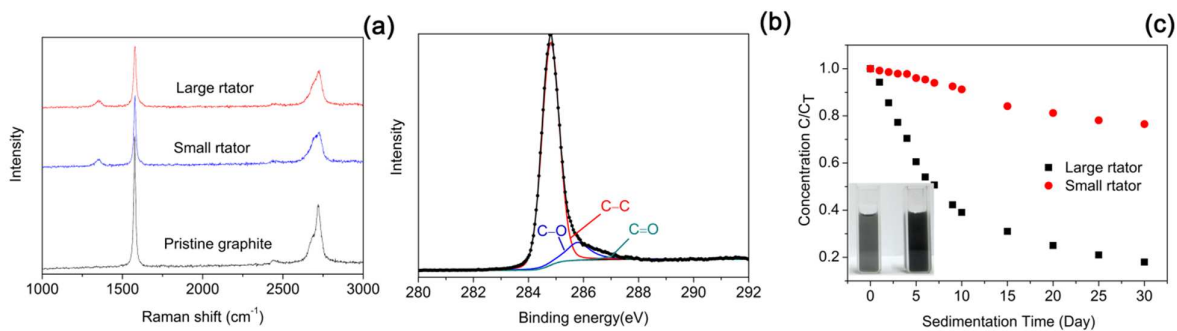
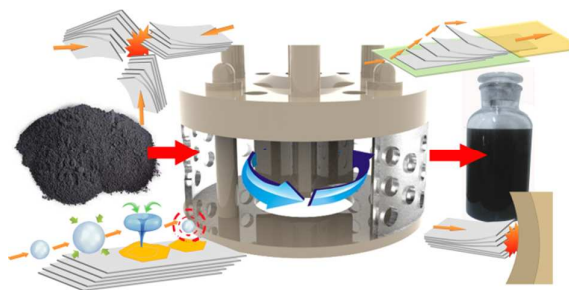


Fig. 5 (a) Raman spectrum of pristine graphite particles and GNSs which are prepared with large and small stators, respectively. (b) XPS spectra of graphene nanosheets prepared by high shear mixer with small stator. (c) Sedimentation curves for GNSs dispersion prepared with large and small stators. C/C_T is the ratio of the real-time concentration to the initial concentration. Inset: the photograph of GNSs dispersions with the same concentration stood for a week under ambient conditions.

ToC figure :



The synergistic enhancement of shear forces and collision effects can result in an effective exfoliation of ultrathin graphene nanosheets.

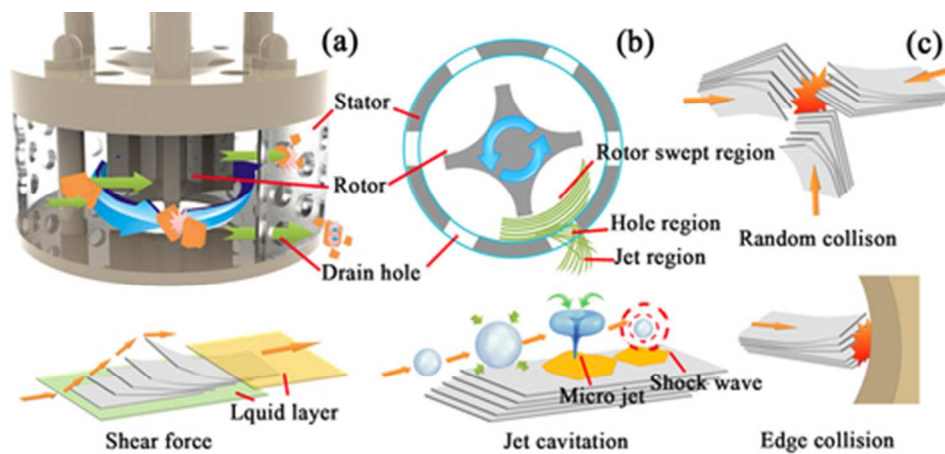


Fig. 1 (a) 3D sectional drawing of the high shear generator; (b) Main energy dissipation regions of the high shear mixer (sectional view); (c) The schematic model of preparing GNSs by shear force, collision and jet cavitation.

40x19mm (300 x 300 DPI)

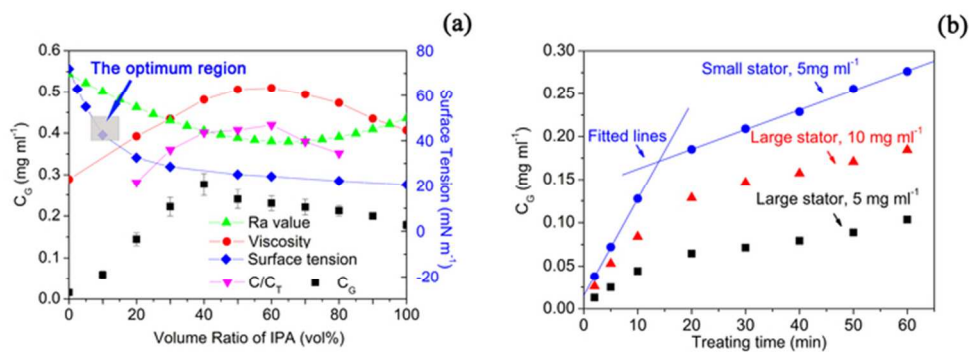


Fig. 2 (a) Graphene concentration (CG), viscosity, surface tension and Ra value of IPA-water mixtures with different volume fraction. The grey area presents the optimum region of surface tension. C/C_T is the residual concentration after standing for one month to the initial concentration. (b) The concentration of GNSs dispersion prepared with different stators in 40 vol % IPA-mixtures. Fitted lines of CG show the different growth rates in the initial and relatively steady phases.

31x11mm (600 × 600 DPI)

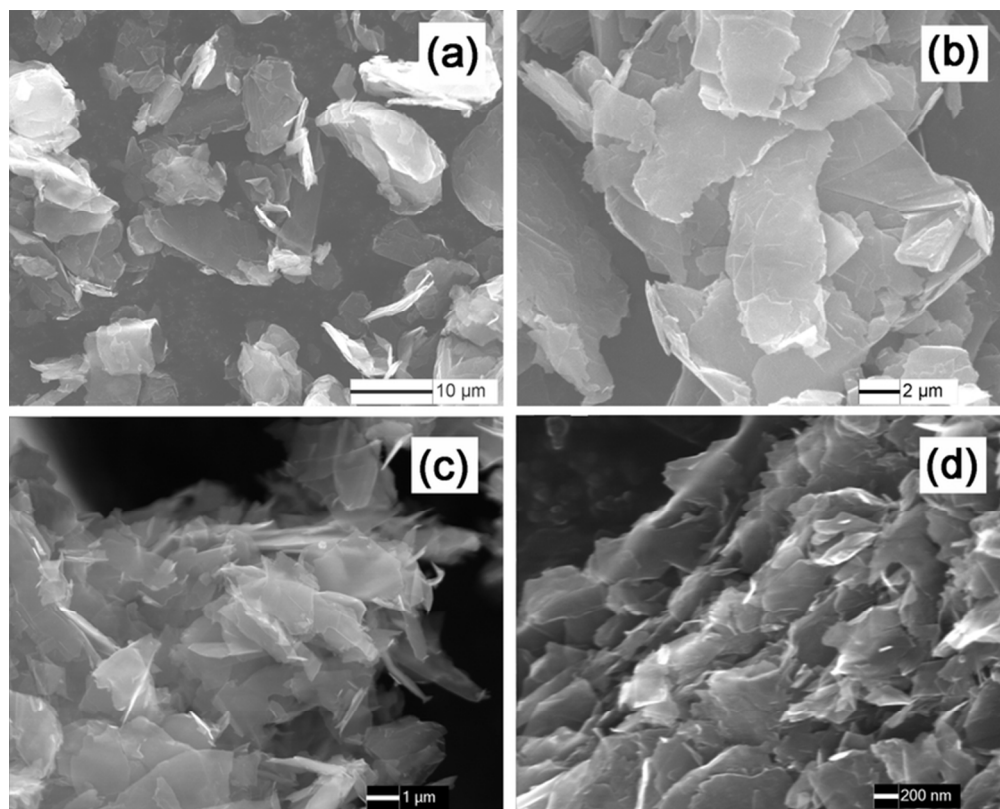


Fig. 3 SEM images of (a) pristine graphite particles, (b) the sediment. FESEM image of GNSs prepared with (c) the large and (d) the small stators.
68x54mm (300 x 300 DPI)

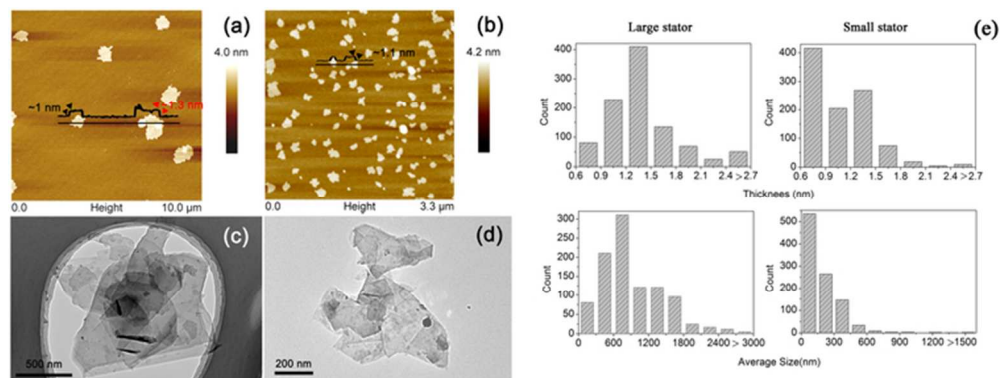


Fig. 4 AFM and TEM images of GNSs prepared with (a, c) large and (b, d) small stators. To avoiding the loss of small flakes through the holes in the holey carbon grid, the small stator sample was prepared in ultrathin carbon support film. (e) Statistical analysis of AFM images showing histograms of thickness and flake average size for GNSs dispersion prepared with large and small stators.
64x24mm (300 x 300 DPI)

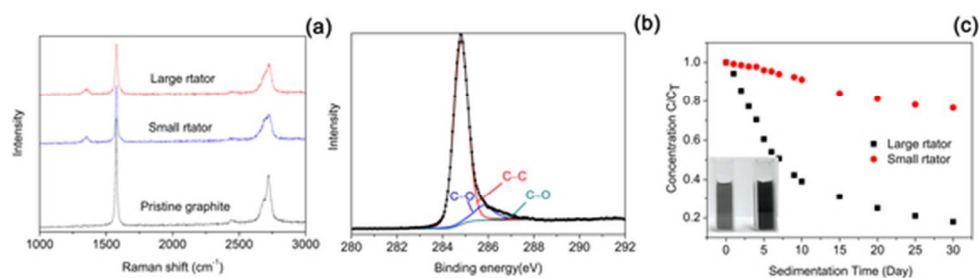
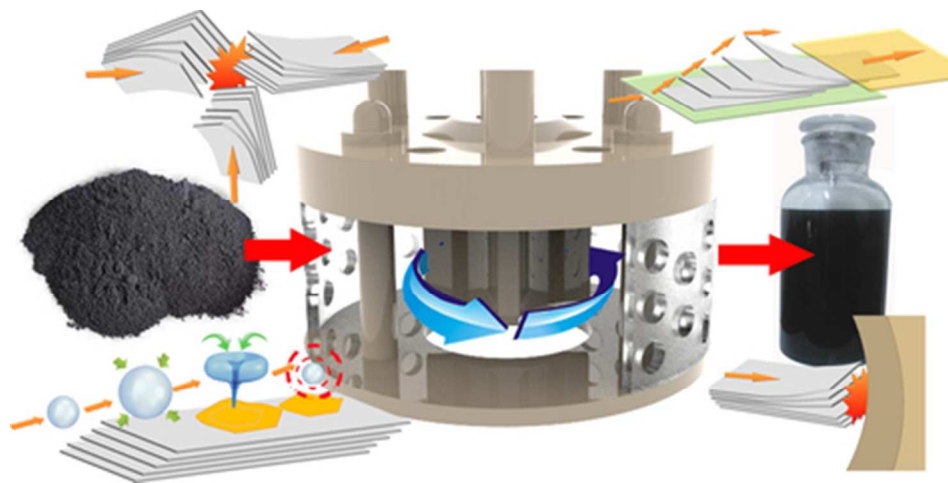
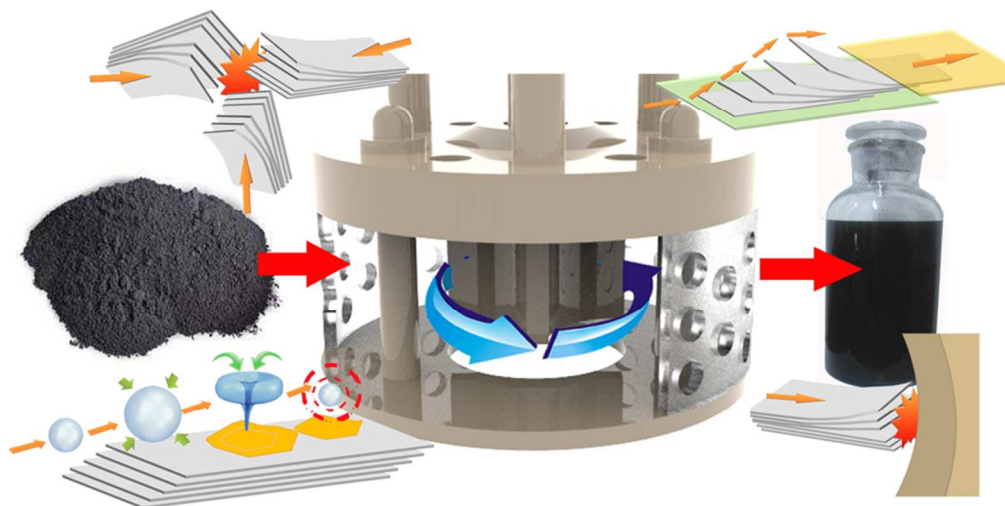


Fig. 5 (a) Raman spectrum of pristine graphite particles and GNSs which are prepared with large and small stators, respectively. (b) XPS spectra of graphene nanosheets prepared by high shear mixer with small stator. (c) Sedimentation curves for GNSs dispersion prepared with large and small stators. C/C_0 is the ratio of the real-time concentration to the initial concentration. Inset: the photograph of GNSs dispersions with the same concentration stood for a week under ambient conditions.
50x14mm (300 x 300 DPI)



39x19mm (300 x 300 DPI)



The synergistic enhancement of shear forces and collision effects can result in an effective exfoliation of ultrathin graphene nanosheets.
80x39mm (300 x 300 DPI)